

## Ultrathin entirely flat Umklapp lenses

Gregory J. Chaplain<sup>1</sup> and Richard V. Craster<sup>1,2</sup>

<sup>1</sup>*Department of Mathematics, Imperial College London, London SW7 2AZ, United Kingdom*

<sup>2</sup>*Department of Mechanical Engineering, Imperial College London, London SW7 2AZ, United Kingdom*



(Received 9 January 2020; revised manuscript received 6 April 2020; accepted 7 April 2020; published 28 April 2020)

We design ultra-thin, entirely flat, dielectric lenses using crystal momentum transfer, so-called Umklapp processes, achieving the required wave control for a new mechanism of flat lensing; physically, these lenses take advantage of abrupt changes in the periodicity of a structured line array so there is an overlap between the first Brillouin zone of one medium with the second Brillouin zone of the other. At the interface between regions of different periodicity, surface, array guided waves hybridize into reversed propagating beams directed into the material exterior to the array. This control, and redirection, of waves then enables the device to emulate a Pendry-Veselago lens that is one unit cell in width, with no need for an explicit negative refractive index. Simulations using an array embedded in an idealized slab of silicon nitride ( $\text{Si}_3\text{N}_4$ ) in air, operating at visible wavelengths between 420–500 THz demonstrate the effect.

DOI: [10.1103/PhysRevB.101.155430](https://doi.org/10.1103/PhysRevB.101.155430)

### I. INTRODUCTION

Inspired by the ability to create flat lenses, such as the Pendry-Veselago lens [1], there has been a drive towards developing flat optical devices to manipulate light [2,3]. Advances in metasurface-based technologies paved the way for these planar devices, with realizations in a variety of settings, operating by several different modalities. These operational regimes include plasmonic waveguide structures [4], i.e., bulk materials composed of alternating metal-dielectric layers [5], or all dielectric inhomogeneous layered lens antennas [6]. Alternate flat lens devices focus on controlling abrupt phase changes endowed to incident wavefronts upon transmission [7,8], taking advantage of gradient index structures [9], or by manufacturing protruding subwavelength elements, enabling generalized refractive laws to be observed [2].

Less exotic materials which achieve anomalous refractive phenomena are photonic crystals (PCs). These structures exert their control over electromagnetic radiation through effects, such as Bragg scattering, which arise due to their periodic structure, allowing all angle negative refraction to be achieved [10] without the existence of simultaneously negative effective permittivity and permeability, which is the case in metamaterials [1]. All-angle negative refraction, together with restoring evanescent wave components, is the hallmark of the perfect lens [1]. Either or both aspects have been used in PC devices to enable superresolution [11–13]. Unlike conventional metalens or diffractive lenses [14], here we present a new, novel, flat dielectric lens antenna (DLA) device based on simple *one-dimensional* periodic structures, with positive permittivity and permeability, operating in narrow frequency bands over the frequency range 420–500 THz. These devices operate by promoting Umklapp scattering [15] at a designed region, and offer a new, unconventional, modality of flat lensing, as shown in Fig. 1 and demonstrated in Fig. 2. The proposed structures act to *emulate* negative refractive effects;

no superresolution is achieved as we do not reconstruct any evanescent wavefields or use resonant materials. As such the proposed devices mimic only one property of the perfect lens, and can be considered a new type of “poor man’s superlens.”

A thorough review of anomalous refractive effects in two-dimensional photonic crystals [16] outlines the techniques in analyzing isofrequency contours, or wave-vector diagrams, of periodic media, enabling the design of simple photonic crystals with remarkable refractive properties, taking use of *Umklapp* refracted beams. We will focus on this scattering mechanism throughout the article, elucidating on nuances that arise when interpreting periodic media, particularly in terms of crystal momentum transfer. The advantages, if any, of studying simpler one-dimensional (1D) periodic structures are not immediately apparent as compared to their two-dimensional (2D) counterparts; many effects in 2D photonic crystals arise due to the periodicity in both directions. For 1D structures, analysis has only been concerned with cases that have interfaces chosen *along* the stacking direction (the direction of periodicity), which is the only symmetry direction for the 1D grating system [16,17]. A clear advantage of 1D devices is that they are substantially thinner, but would require the ability to manipulate waves propagating *with* the periodic direction. In this article we show that not only is this possible, but it is also effective in creating new unconventional lensing applications, through promoting crystal momentum transfer.

When dealing with periodic media, analysis in reciprocal space via the Brillouin zone (BZ) [18] is invaluable. To understand, predict, and interpret the existence and direction of any refracted beams at the interfaces involving periodic media, isofrequency contours (wave-vector diagrams) are used [19]; these contours offer simplistic yet powerful insight into interactions within periodic media. An important concept is that the Bloch wave vectors in a periodic structure are defined up to a reciprocal lattice vector  $\mathbf{G} = 2\pi/a$ , with  $a$  the width of the unit cell. Band folding interpretations are commonly

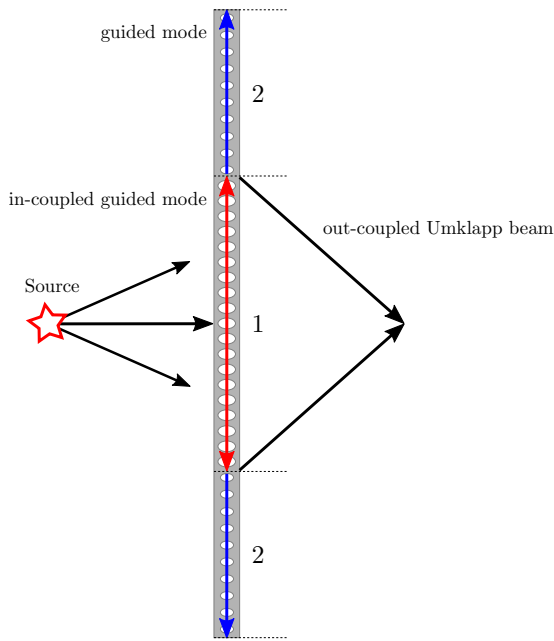


FIG. 1. Umklapp scattering mechanism yielding negative refraction and focusing. A source incident on region 1 of the device excites an in-coupled (leaky) guided mode (red arrow). This propagates to regions 2, where the periodicity is abruptly changed. Similar guided modes are excited in these regions (blue arrows), along with transfer of crystal momentum via Umklapp scattering, resulting in out-coupled, backwards-bended, Umklapp beams.

used to infer higher-order interactions within periodic media, as a direct consequence of the Floquet-Bloch nature of the waves; in periodic media, wave vectors define a superposition of plane waves through Bloch's expansion. As a consequence the phase of the envelope wave, which carries fast oscillatory solutions, lies within the first Brillouin zone [16,20,21]. Conserving the sum of reduced wave vectors leads to descriptions of such interactions by the addition of a phase factors, or phase-matching conditions [22], due to the periodicity of the medium and nature of the Bloch solutions it supports. Throughout this article we will promote Umklapp scattering to convert surface guided waves into backward-bent propagating bulk modes by physically exploiting anharmonicity within the lattice; we design an abrupt transition in periodicity within a one-dimensionally periodic dielectric waveguide. Using this technique allows focusing of energy to be achieved, and as such we term the presented devices Umklapp lenses.

There is a long history of controlling waveguide modes in 1D periodic structures, particularly through anomalous refraction and, notably, light propagation in planar waveguides is extensively investigated in [23]. The structures we consider, and subsequent analysis, is similar to that presented in [23], in that we design 1D periodic waveguides using wave-vector diagrams. There are, however, some important distinctions between previous work and the new devices we design. To highlight these we compare our device to the 1D periodic corrugated plane waveguide in [23], with the distinctions outlined in Fig. 3. First, typical 1D periodic devices are extended in the orthogonal direction to the periodicity (in the plane of the device), providing a long interaction length for so-called

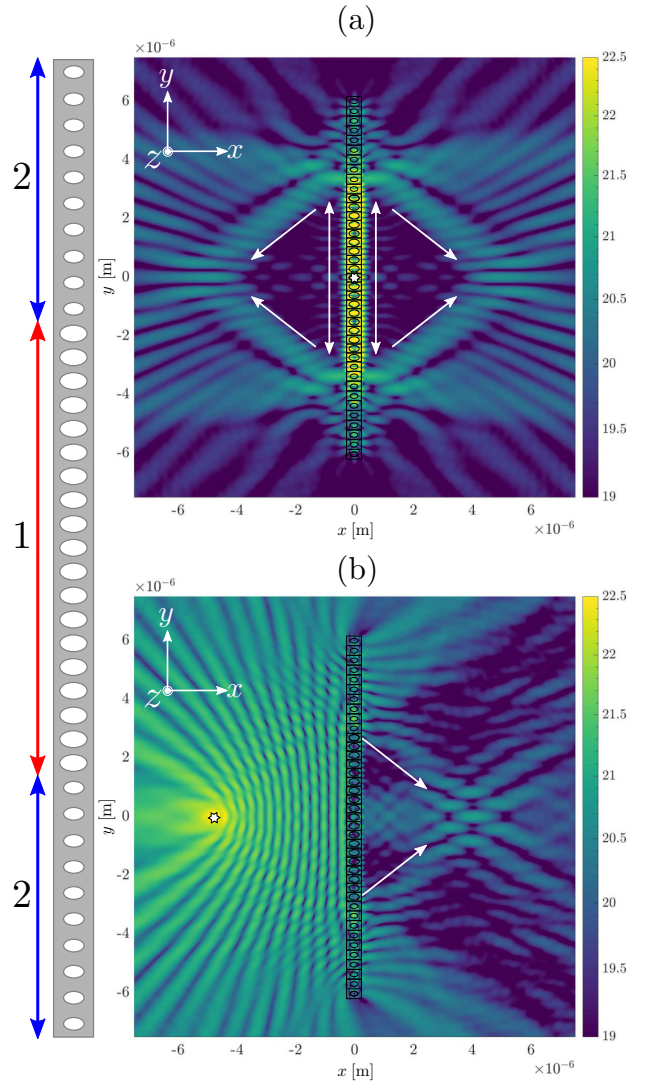


FIG. 2. Dielectric thin flat lens (2D simulation): logarithm of electric field  $\log(|E_z|)$  (arbitrary units), perpendicular to the page, excited by current line source, marked at white star operating at frequency 484THz. (a) Array centered source, giving reversed conversion via the Umklapp mechanism. (b) Flat lensing by source placed at  $-8\lambda$ , producing image at opposite focal spot. The array is shown on the left: device length is  $L = 12.3 \mu\text{m}$ , with width  $w = 500 \text{ nm}$ , and infinite in  $z$ . The maximum amplitude in each focal spot in (a) is  $\sim 10\%$  of the source amplitude.

phase matching conditions to occur. In the devices we consider, the orthogonal direction is very much finite with respect to the direction of the periodicity, i.e., there are no propagating modes in the orthogonal direction. Second, to ensure efficient coupling tapered, or graded, regions are used in corrugated waveguides. Contrary to this we have *no* grading. We are in fact utilizing, indeed advocating, Umklapp scattering at a region of abrupt transition in periodicity. Third, the corrugated guide has only one periodicity, the region in reciprocal space where coupling to directed waves is efficient is local to the band edge (of the first Brillouin zone), and is only achieved by means of Bragg scattering. By designing, as we do here, two

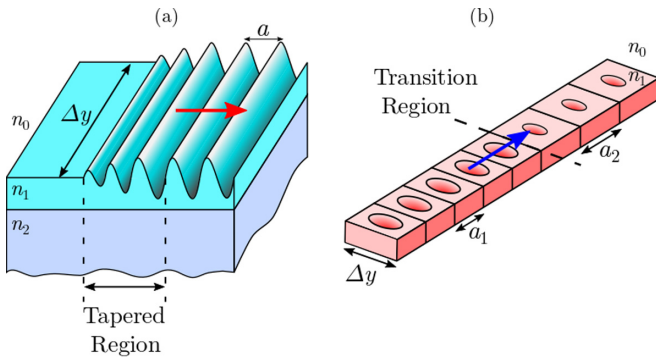


FIG. 3. Comparison between conventional 1D periodic grating structures, with differing refractive indices shown as  $n_i$ , as in [23] (a) and the presented Umklapp devices (b). (a) Shows a 1D periodic corrugated device, with the periodicity  $a$ , shown. Prior to this region is a tapered region. This is not present in (b), showing a portion of the Umklapp lens, as an abrupt transition region is used between the *two* differing periodicities  $a_1, a_2$  (the simulations throughout the article are considered for a similar device, but infinite in the  $z$  direction). Further to this, in the orthogonal direction to the periodicity, the spacing  $\Delta y$ , in the grating case is such that  $\Delta y \gg a$  to provide a long interaction length. This is not the case for the Umklapp devices, where  $\Delta y \sim a$ . Finally, the red arrow in (a) shows the direction, perpendicular to the grating interfaces, in which no refractive effects can be achieved [23]. The same direction is shown in (b) in blue, where the effects are *maximally* achieved.

regions of differing periodicity we are able to move further away from the edge of the BZ in reciprocal space; coupling between different order frequency bands of the geometrically distinct regions permits operation at several frequencies. This is achieved by the transfer of crystal momentum, emphasizing the attribution to the Umklapp mechanism. Fourth, and perhaps most pertinent, is that in conventional periodic structures “cross coupling is a special property of wave propagation at oblique angles with respect to the grating, it cannot exist for waves at normal incidence to the grating lines [23].” We show here that our structures have *maximal* coupling with back-banded propagating modes for guided waves which propagate at normal incidence to the grating lines/periodic direction.

The ability to excite counterpropagating modes in coupled periodic waveguides by phase matching arguments is well established [24], as is leveraging momentum transfer for negative refraction effects [25]. However, the Umklapp devices presented here possess a certain novelty in that the conversion takes place not only in the opposite direction, but from a guided surface mode to a propagating beam, all through promoting Umklapp scattering at a desired region.

The design of structures capable of supporting guided surface modes is not limited to the field of optics. Recent design paradigms for adiabatically graded arrays have resulted in a remarkable level of wave control, and phenomena being observed, in multiple disciplines within wave physics stretching beyond electromagnetism, from elastic vibrations to acoustics. The inspiration of many such designs stem from the rainbow trapping effect, originating in electromagnetism [26], whereby the speed and phase of localized array guided modes is manipulated by graded geometrical changes of the

array components. Elementary resonant, often subwavelength, devices were proposed [27,28], and built [29], for elastic media enabling trapping, and mode conversion transferring energy from surface to body waves, effects for array guided surface states for applications to energy harvesting [30] from vibration. Recently, a reversed conversion phenomena which emulates negative refraction by a line array [31] was developed using a counterintuitive effect hybridizing both trapping and conversion; this relies upon band crossings and phase matching all within the first Brillouin zone and uses adiabatic grading of an array all in the setting of elastic waves.

In this article we propose a much more versatile design paradigm employing Umklapp “flip-over” processes to achieve flat lensing. Despite its origins in thermal transport, we can readily adapt the Umklapp mechanism for our dielectric structures since they are periodic; these processes are inherent to any system permitting Floquet-Bloch waves. The operation rests on the segregation of the device into structured regions of different periodicities, thereby creating two different Brillouin zones in reciprocal space, and the subsequent analysis of the corresponding dispersion curves. Contrary to the adiabatically graded arrays considered in [31], there is no grading between the regions but instead an abrupt change in the array periodicity; undesirable scattering of the field at such an interface is anticipated, but by carefully engineering the design we can recapture the scattered field by promoting Umklapp processes thereby providing a remarkably simple way to achieve flat lensing, without the need for exotic materials or inhomogeneities.

We consider the full, three-component time harmonic electric fields  $\mathbf{E}$  using the finite element method (FEM) with COMSOL multiphysics [32] to solve the equation

$$\nabla \times (\mu_r^{-1} \times \mathbf{E}) - k_0^2 \left( \epsilon_r - \frac{j\sigma}{\omega\epsilon_0} \right) \mathbf{E}, \quad (1)$$

where  $\mu_r$  and  $\epsilon_r$  are the relative permeability and permittivity tensors, respectively,  $\epsilon_0$  is the vacuum permittivity,  $k_0$  is the free space wave number,  $\sigma$  the conductivity, and  $\omega$  the angular frequency. For the purely dielectric devices considered throughout,  $\mu_r = 1$  and  $\sigma = 0$ . We focus on localized guided electromagnetic waves confined to a dielectric slab in air, choosing silicon nitride  $\text{Si}_3\text{N}_4$  as the dielectric as it is widely used in applications due to its high relative permittivity ( $\epsilon_r = 9.7$ ), ubiquity in integrated circuitry [33] and transparency over the visible range in nanoengineered structures both with low contrast ( $n \approx 2$ ) and loss [34]. Throughout this article we will work with an idealized slab of  $\text{Si}_3\text{N}_4$ , whose properties are assumed to be frequency independent, as such  $n = \sqrt{\epsilon_r \mu_r}$ , since the important characteristics arise from the periodicity of the structure (and not its composition). The supported guided states manipulated throughout are neither surface plasmon polaritons, or their spoof counterparts [35,36] since we do not deal with opposing signs of permittivities or structured metallic interfaces. Indeed the proposed structuring takes place within the device, leaving its edges completely flat (Fig. 4). As such we are free to model these devices efficiently in air operating in the terahertz frequency range; the corresponding device dimensions are achievable in waveguide technologies [37,38]. We do not exploit resonance effects, and so the imaging is not subwavelength, yet the proposed DLA

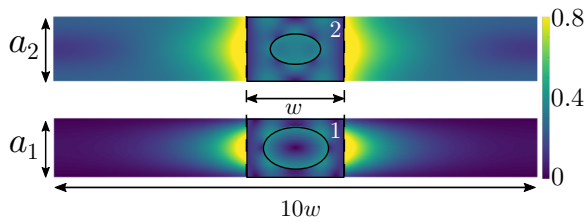


FIG. 4. Typical electric fields, of similar mode symmetry, as  $|E|$  for each regions 2(1) with unit cells  $a_{2(1)}$ . Elliptical inclusions have semi-major and minor axes  $r_a$  and  $r_b$ , respectively, detailed in Table I. FEM method and boundary conditions are shown in Supplemental Fig. S3 [41].

devices, are ideal for demonstrating the efficacy of Umklapp scattering.

Our analysis of where (spatially) and how Umklapp mechanisms can be exploited to produce back-bended reversed beams is, theoretically, independent of the material and device size and rests upon exploiting the dispersion curves and isofrequency contours of the different periodicities within the device, as detailed in Sec. II. The performance of the device as a flat lens, however, is strongly dependent on the sizes of the constituent regions, as demonstrated in Sec. III. The methodology can be readily extended for dielectric coatings or substrates, i.e., the device does not have to have identical media on either side. Using this, we then outline how to harness this promoted scattering effect to generate a new mechanism for flat lensing, and investigate the effects of losses in the device. Suitable scaling to other materials, and sizes, permits the tunability of the frequency bandwidth, leading to a new operational capacity for dielectric substrates.

## II. DESIGN METHODS

When analyzing periodic media it is naturally convenient to display the dispersion diagrams of such materials within the irreducible Brillouin zone (IBZ) [18]. Conventionally, we concentrate upon modes below the dispersionless light line of free space waves, that is, within the first BZ; Umklapp processes, arising due to the transfer of crystal momentum from higher BZs, are often thereby ignored. We demonstrate that there are advantages in using these processes by considering two regions of differing periodicities within the same dielectric array, such that there is an overlap between the first BZ of one periodic region and the second BZ of the other. At the abrupt transition between these regions Umklapp scattering is dominant and reversed conversion can be achieved and utilized for flat lensing.

The Umklapp mechanism, first hypothesised by Peierls in 1929 [15] is conventionally used to describe thermal transport and resistivity of metals at high temperatures, and is now prevalent in the quantum theory of transport [39,40]. It is a manifestation of the transfer of crystal momentum within the system, and exploits the fact that in periodic media wave vectors are defined up to a reciprocal lattice vector  $\mathbf{G} \equiv 2\pi/a$ , with  $a$  being the periodicity of the unit cell. Thus in the case of scattering two initial wave vectors, say,  $\mathbf{k}_1, \mathbf{k}_2$  then if the resultant  $\mathbf{k}_3$  lies beyond the first Brillouin zone it experiences the

	Region 1	Region 2
$a$	300nm	330nm
$w$	500nm	500nm
$r_a$	110nm	80nm
$r_b$	170nm	130nm

Table I: Parameters within dielectric slab; region 1(2) coloured red(blue) in Fig 7(g) ( $z$ -direction taken to be infinite.)

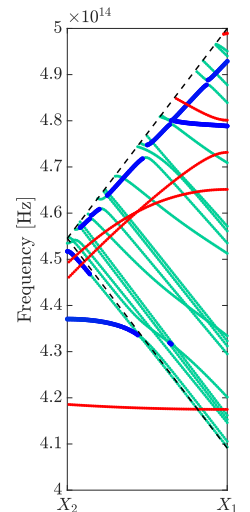


FIG. 5. Dispersion curves for region 1 (2) in red (blue), plotted from  $X_2$  to  $X_1$ , i.e., in the second BZ of region 2 while in the first of region 1. The dashed line represent the dispersionless light line, with the “folded” light line also shown. Matching mode shapes promotes U-processes. Full dispersion curves, and domain probe method used to eliminated spurious modes (green curves) are shown in supplemental Fig. S2 [41].

Umklapp, or “flip-over” mechanism via crystal momentum transfer [20]. Two types of scattering processes are defined: normal (N-processes) and Umklapp (U-processes) through

$$\mathbf{k}_1 + \mathbf{k}_2 - \mathbf{k}_3 = \begin{cases} \mathbf{0} & \text{N-process,} \\ \mathbf{G} & \text{U-process.} \end{cases} \quad (2)$$

This mechanism has recently been observed to cause excess resistivity in graphene [42] and used to explain the coupling of acoustic and optical branches in crystals [43]. We apply it, for the first time, in a flat lensing scenario, circumnavigating any ambiguities considered with Umklapp scattering [20], by adopting the conventional description in Eq. (2), analyzing U-processes for scattered wave vectors lying outside the first BZ; this is a natural way to distinguish between N- and U-processes and is critical in this design process.

For the application of the Umklapp mechanism to localized guided electromagnetic (EM) waves for flat lensing, we partition a dielectric slab into two regions of differing periodicities, see Fig. 1. To set the context, we first analyze a perfectly periodic medium of consisting of a slab of  $\text{Si}_3\text{N}_4$  in air structured with a periodic array of elliptical inclusions with pitch  $a_1$ , with geometrical parameters given as region 1 in Table I as shown in Fig. 4. Then consider the same dielectric material but with the array having a larger periodicity  $a_2$  and different inclusion size (region 2 in Table I). The two regions are defined with unit cells of length  $a_1, a_2$ , respectively, such that  $a_2 > a_1$ . Consequently, the first BZ of region 2 is smaller than that of the region 1. Thus, the edges of the first BZ for the regions,  $X_i \equiv \pi/a_i$ , satisfy  $X_2 < X_1$  and are offset from each other. The dispersion curves within this overlapping region are calculated using the FEM software COMSOL multiphysics and shown in Fig. 5. The frequencies where overlap between the dispersion curves of similar mode shapes are where U-processes take effect efficiently; the excited mode in region 1 must be able to

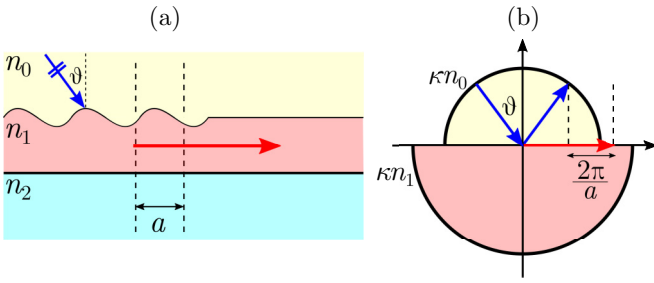


FIG. 6. Conventional mode coupling diagrams, as in [22]. Panel (a) shows a schematic of an incident wave vector (blue arrow) coupling to a waveguide mode (red arrow) through some interaction with a periodic medium, thanks to the transfer of crystal momentum. This is shown in the wave-vector diagram in (b) due to phase matching, which is really a result of crystal momentum transfer.

excite a mode that exists in the region 2, otherwise an effective hard boundary is reached at the transition region, resulting in undesirable scattering; typical fields showing similar modal symmetries in the two regions are shown in Fig. 4. While not a requirement for the transfer of crystal momentum, designing the band crossings to have opposite signs of group velocity enhances the coupling between the surface guided modes and the propagating waves excited by Umklapp scattering [20,40]. This effect is achieved for several of the overlapping bands shown in Fig 5, ranging between 420–500 THz, and therefore has potential for broadband performance. A further example of the reversed conversion effect is shown in supplemental Fig. S1[41].

We now consider the implications of structuring a finite slab of  $\text{Si}_3\text{N}_4$  into two distinct regions, one with the periodicity and unit cell structure of region 1, in Table I, that then transitions abruptly to incorporate the parameters associated with region 2. Conversion of the array guided mode occurs into a beam in the exterior medium that is backward-bent; the angle of the reversed conversion is predicted by inspecting the isofrequency contours of the two regions. Shown in Fig. 7 are simplistic isofrequency contours for the respective components of the dielectric slab; we show for clarity the isofrequency contour of each medium as a circle, acknowledging that it, in fact, corresponds to a point on the  $\kappa_x$  axis when projecting the dispersion curves into wave-vector space. This is how wave-vector diagrams are historically used when the device dimensions in the orthogonal direction to the periodicity are large [23], as such the periodicity acts to modulate the free-space wave-vector diagrams. Despite our devices not having any propagating components in the orthogonal direction to the periodicity, we adopt this picture for familiarity and clarity. Exploiting the coupling at a sharp change in periodicity is inspired by conventional diffractive mode coupling theory [22]; incident radiation of wave vector  $\kappa$  in a media with refractive index  $n_0$ , is coupled to a waveguide mode of vector  $\kappa_{wg}$  through phase matching by incorporating the periodicity, such that

$$\kappa_{wg} = \kappa n_0 \sin \theta + \Lambda, \quad (3)$$

where, for integer  $m$ ,  $\Lambda = 2m\pi/a$ . This is shown in Fig. 6. Using this mode-coupling picture we can interpret the

hybridization mechanism from the “contours” of the medium composed of differing periodicities; while the following resembles this diffractive theory, the mechanism is fundamentally achieved through Umklapp processes by *crystal momentum transfer*. The coupling *into* the waveguide by gaining momenta of multiples of  $\mathbf{G}$  is therefore distinct to Umklapp processes, in which momenta are subtracted, which leads to the out-coupling into back-bended beams. Understanding both momentum transfer mechanisms is important for the performance of the device in terms of exciting the guided modes on the device and their conversion.

In Fig. 2(a), the array is excited with a source to generate a guided wave with wave vector in region 1. This is shown schematically in Fig. 7(a), with the corresponding wave-vector diagram below. Despite being 1D periodic we show this as a half circle as is customary in these interpretations [22]. The corresponding “contour” is defined within the first BZ such that  $\kappa \in [-\pi/a_1, \pi/a_1] \equiv [-X_1, X_1]$ . At a designed spatial position, we then abruptly change the periodicity to that of region 2, marked by the schematic of the blue region in Fig. 7(b). Below this shows the corresponding wave-vector diagram where the length of the wave vector is the same as in Fig. 7(a) as we are operating at the crossing of two supported dispersion curves; the material properties have not changed, only the geometry has altered. At this frequency, the wave vector now lies in the second BZ of region 2 since  $X_2 < \kappa < X_1$ . This is highlighted in Fig. 7(c), by drawing a “band folded” version of the contour describing this wave vector. This is actually formed by translating every point outside the first BZ by  $\mathbf{G} = 2\pi/a_2$ . The critical observation is that this initial wave vector, marked by the red arrow, experiences a transfer of *crystal momentum* via the Umklapp effect, resulting in the translation of a collinear reciprocal lattice vector  $\mathbf{G}$ , denoted by the folded isofrequency contours. The resultant flipped vector is shown in Fig. 7(d). Shown in Fig. 7(e) is the superimposed isofrequency contour of the exterior medium (in this case, air) that surrounds the array (yellow circle). Phase matching, by conserving the tangential component of the flipped vector, with this contour gives the resultant scattered wave vector that, in turn, predicts the reversed conversion angles as in Fig. 2(a). Since the device is surrounded by air on either side, there are two beams shed with equal angle, highlighted in the compact diagram in Fig. 7(f), with a schematic shown in Fig. 7(g). The wave vector components of Fig. 2(a) are seen in the Fourier spectrum shown in Fig. 8, corroborating the adopted wave-vector diagram analysis.

We stress that this methodology is completely general, and as such the device can have different media on either side of the interfaces, raising the possibility of different angles of reversed conversion on either side. As such there is a broad range of applications for these structures as dielectric coatings, capable of mimicking generalised lenses [44]. The angle is explicitly predicted from mode-coupling analysis by rearranging Eq. (3) to incorporate the effect of the second periodic region; in this setting  $\Lambda = 2\pi/a_2 > \kappa_{wg}$ . Thus we can generalize conventional mode-coupling techniques for a wave confined to the array arriving at a region with altered periodicity and notably U-processes provide coupling to the first *negative* diffractive order of mode coupling theory [22].

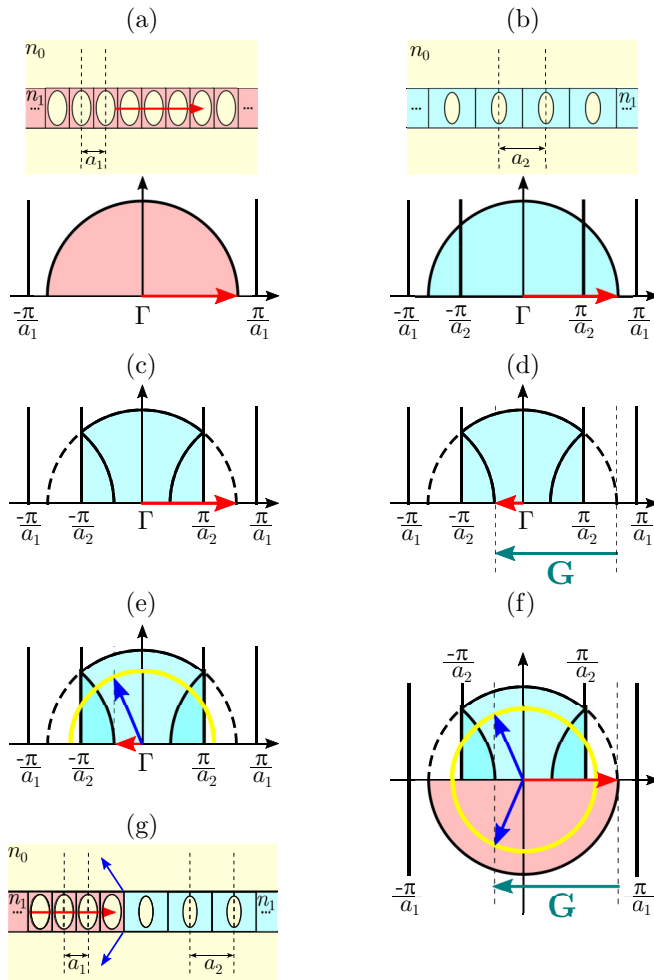


FIG. 7. Step-by-step wave-vector diagrams. Panels (a, b) show schematics of the two periodic regions, with the corresponding wave-vector diagrams below. Each has the same length of incident wave vector, which lies in different BZs depending on the periodicity, shown by the BZ boundaries  $\pm\pi/a_{1,2}$ , respectively. Panel (c) shows a band folded, or irreducible, picture by translating points outwith the first BZ of region 2 by a reciprocal lattice vector  $\mathbf{G} = 2\pi/a_2$ . Panel (d) shows the resultant wave vector after Umklapp scattering takes place through the transfer of crystal momentum. Panel (e) shows the conserved wave vector by phase matching with the isocircle of the free space surrounding the device. Panel (f) shows the previous five wave-vector diagrams superimposed into a compact diagram which allows for the prediction of the angles of the reverse converted waves. Panel (g) shows a schematic of the process.

By (a)symmetrically introducing abrupt changes in periodicity about a central point, we can image a line source on the array to two focal spots on either side of the slab, as in Fig. 2(a), and tune the position of these focal points.

### III. UMKLAPP LENSING

Our arguments also generalize for excitation by a source removed from the array. We again use the Umklapp and the reversed conversion mechanisms at interfaces between different regions of periodicity, but now introduce reciprocity to generate focusing from one side of the slab to the other.

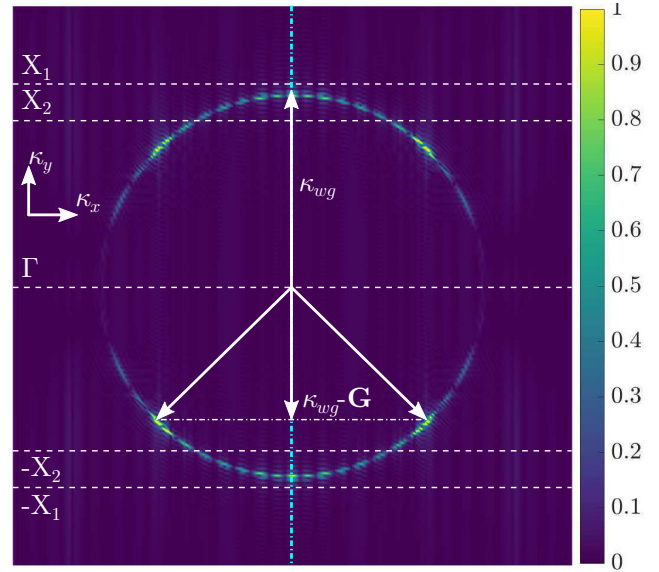


FIG. 8. Fourier transform of Fig. 2(a), normalized to maximum Fourier amplitudes (arbitrary units). The periodicity is understood to be in the direction of  $\kappa_y$  shown. We show one wave-vector component of the initially excited guided mode, namely the vertical wave vector  $\kappa_{wg}$ , lying between  $X_2$  and  $X_1$ . This is flipped by Umklapp scattering to the negatively pointing  $\kappa_{wg}-\mathbf{G}$ , with respect to  $\Gamma$ . Conserving the tangential component of this hybridizes the guided surface waves with counterpropagating bulk waves, shown by the bright spots lying on the isocircle of the free space waves; any wave-vector components which lie off the vertical cyan dashed-dotted line are understood to be propagating waves off the array. The center of the Brillouin zones is shown ( $\Gamma$ ), with the BZ boundaries of region 1(2) highlighted by the dashed lines  $\pm X_{1(2)}$ . This diagram is the scattering-simulation counterpart of Fig. 7(f) obtained from the dispersion relation.

An isotropic current line source is placed at one focus of Fig. 2(a), and an image is produced at the other side of the array, showing the device is capable of emulating negative refraction. The focusing response is due to the horizontal wave component igniting the surface guided wave, which propagates along the dielectric array to the regions of altered periodicity, seen in Fig. 2. Upon reaching these altered regions, Umklapp scattering takes place and the reversed conversion effect acts to refocus this point source on the opposite side of the device, as clearly shown in Fig. 2(b). The device then acts as a lens in the sense that it can focus incoming radiation at a given focal point. Unlike conventional lenses, changing the source position will not alter the focal spot position; the flexibility in the positioning of the focal spots is, however, achieved through altering the position of the transition regions, the relative periodicities, frequency of excitation, and symmetry. This effect only takes place due to the transfer of crystal momentum and as such we term these devices Umklapp lenses.

The position of the source position does, however, unlike in classical lenses, affect the performance of the structure. This can be seen in Fig. 9, where we analyze the performance of the Umklapp lens compared to two other structures; a plain dielectric slab and a dielectric slab which is only patterned with the periodicity and inclusions of region 1. The position

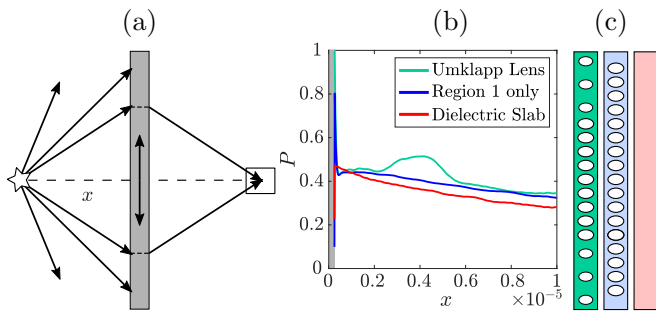


FIG. 9. Performance of device with respect to horizontal distance of source. Panel (a) shows schematic of the setup where the source position (star) is gradually placed further from the device, along the center line. The performance  $P$  is measured by integrating the electric field  $|\mathbf{E}|$  over a region encapsulating the focal spot predicted from Fig. 2 (rectangular box). Panel (b) shows the power in this region for three types of material: the Umklapp lens (green), a dielectric slab patterned only with Region 1 (blue) and a blank slab (red), normalized to the maximum performance of the Umklapp lens. The optimal focal distance away from the device edge (shown as grey region) for the Umklapp lens corresponds to the focal length. Panel (c) shows schematics of the tested devices.

of the source is altered along the line which perpendicularly bisects the device. The performance is analyzed by integrating  $|\mathbf{E}|$  over a region surrounding the focal spot predicted from the device size and angles of the reversed conversion [Fig. 9(a)]. Exciting very close to the device couples most efficiently the near vertical wave-vector components, parallel to the direction of the periodicity, contrary to other 1D periodic grating devices [23]. Increasing the distance of the source from the center line of the device initially decreases the performance, until the source is placed near the focal length of this frequency. In the vicinity of the focal length, focusing is enhanced on the opposite side of the device [Figs. 2(b) and 9] due to the additional coupling of the wave-vector components incident on the transition region, by reciprocity. As such, unlike conventional “poor man’s superlenses,” these devices have scope for emulating negative refraction in the far field, as this focal length for this frequency is  $\sim 8\lambda$  [45].

Past this point, a critical angle is reached such that there is very little coupling between the propagating wave-vector components of the source with region 1. As such, the focusing capabilities of the device are limited, depending on the source position and the length of the central region 1.

Considering the fabrication of such devices atop other structures, as is conventional in dielectric waveguides [37], also permits tunability of the focal lengths on either side of the device [31]. This, in turn, would effect the optimum source positions for focusing within each of the media. Improvements in the limitation of the device can be made by the periodic structuring of the lens surface, at the cost of it no longer being entirely flat; more propagating wave-vector components can contribute to the guided surface modes by an initial transfer of momentum from the periodic structuring [46].

The validity of this concept for devices is further tested by the introduction of losses within the material, through the addition of an imaginary component to the permittivity. An example is shown in Fig. 10, where the field strength along

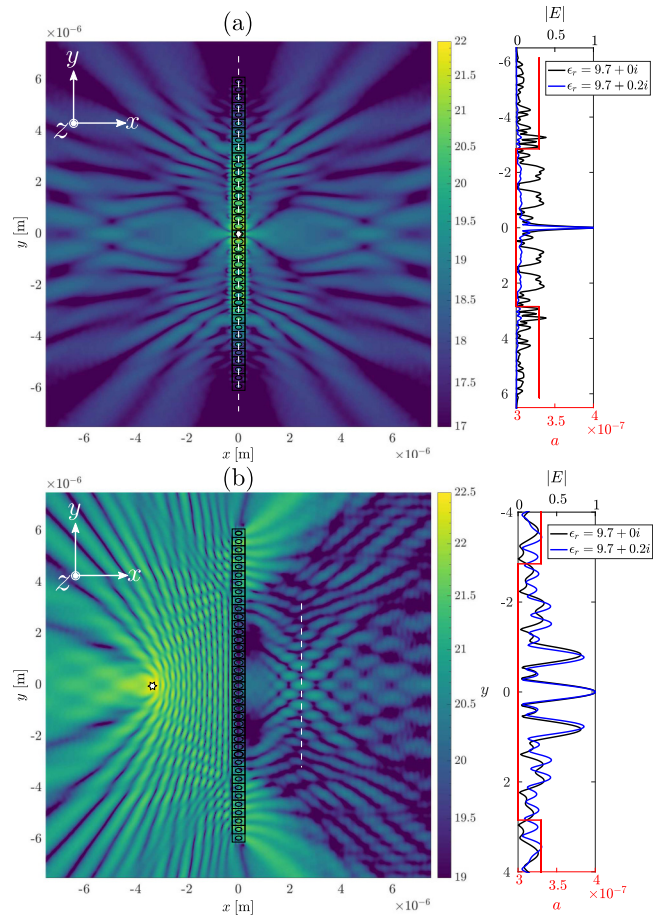


FIG. 10. Same configurations and frequency as in Fig. 4, showing logarithm of electric field,  $\log(|E_z|)$ , for the case with losses introduced with  $\epsilon_r = 9.7 + 0.2i$ . Side panels show comparisons of normalized electric field norm between lossless (black) and lossy (blue) media, plotted along the dashed white lines. Local periodicity  $a$  as a function of position is shown (red). Losses reduce the field strength along the array in (a), while showing that the lossy lens (b) preserves the point spread function.

the center of the devices is compared with, and without, loss for both configurations in Fig. 2. For a lossy material, there is weaker propagation along the array and so the reversed conversion is not as pronounced; the maximum amplitude at the focal spots is now only  $\sim 2\%$  of the maximum source amplitude. This can be mitigated by designing the position of the transition region to lie closer to the point of excitation, and will influence the materials and dimensions chosen to circumnavigate any losses. For decaying surface waves the effect can still be achieved by incorporating the decay length, which can be predicted through homogenisation techniques [27,31]. Despite this, the point spread function of the focal point in the lossless and lossy case remains practically identical.

#### IV. CONCLUDING REMARKS

We develop the concept of Umklapp lensing by designing an array that requires operation at wave vectors outside the first Brillouin zone, and then manipulating confined surface

waves by utilizing crystal momentum transfer. The resulting electromagnetic radiation generates focal points, using high permittivity dielectrics that are both entirely flat, and ultra thin: Negative refractive effects can therefore be emulated with by a line array with thicknesses of just one unit cell.

Similar to classical “poor man’s superlenses” the devices’ focusing capabilities are optimal for near-field excitation, however, there is scope for far-field focusing capabilities due to the additional coupling from wave-vector components when the source is placed at a focal length. Unlike for true superlenses, no evanescent components are reconstructed and as such the imaging is not subwavelength.

Considering lossy materials motivates the design of the transition region between differing periodicities, which is key to employing the Umklapp effect. So too is choosing the periodicities in such a way as to achieve maximal overlap of mode shapes within the differing Brillouin zones. This methodology can be trivially extended to finite 3D devices,

although an extra degree of freedom presents itself in an electromagnetic setting as the relative polarizations of the guided leaky modes become important. As such these devices have the capability of acting as polarization selective Umklapp lenses. At present the proposed devices are purely passive, but there is scope to achieve active components by utilising piezoelectric materials to alter the periodicities and as such, in theoretically demonstrating this new lensing mechanism, we envisage motivation towards experimental verification.

## ACKNOWLEDGMENTS

The authors thank the UK EPSRC for their support through Program Grants No. EP/L024926/1 and No. EP/T002654/1, and a Research Studentship. R.V.C acknowledges the support of the Leverhulme Trust and of the European Union FET Open, Grant No. 863179, Boheme. The authors also thank Yao-Ting Wang for helpful conversations.

- 
- [1] J. B. Pendry, *Phys. Rev. Lett.* **85**, 3966 (2000).
- [2] N. Yu and F. Capasso, *Nat. Mater.* **13**, 139 (2014).
- [3] P. Lalanne and P. Chavel, *Laser Photonics Rev.* **11**, 1600295 (2017).
- [4] E. Verhagen, R. de Waele, L. Kuipers, and A. Polman, *Phys. Rev. Lett.* **105**, 223901 (2010).
- [5] T. Xu, A. Agrawal, M. Abashin, K. J. Chau, and H. J. Lezec, *Nature* **497**, 470 (2013).
- [6] M. K. T. Al-Nuaimi, W. Hong, and W. X. Zhang, in *2014 International Workshop on Antenna Technology: Small Antennas, Novel EM Structures and Materials, and Applications (iWAT)* (IEEE, 2014), pp. 277–280.
- [7] M. Khorasaninejad, W. T. Chen, R. C. Devlin, J. Oh, A. Y. Zhu, and F. Capasso, *Science (NY)* **352**, 1190 (2016).
- [8] P. Genevet, F. Capasso, F. Aieta, M. Khorasaninejad, and R. Devlin, *Optica* **4**, 139 (2017).
- [9] Y. Jin, R. Kumar, O. Poncelet, O. Mondain-Monval, and T. Brunet, *Nat. Commun.* **10**, 143 (2019).
- [10] C. Luo, S. G. Johnson, J. D. Joannopoulos, and J. B. Pendry, *Phys. Rev. B* **65**, 201104(R) (2002).
- [11] C. Luo, S. G. Johnson, J. D. Joannopoulos, and J. B. Pendry, *Phys. Rev. B* **68**, 045115 (2003).
- [12] R. Moussa, S. Foteinopoulou, L. Zhang, G. Tuttle, K. Guven, E. Ozbay, and C. M. Soukoulis, *Phys. Rev. B* **71**, 085106 (2005).
- [13] X. Wang, Z. Ren, and K. Kempa, *Opt. Express* **12**, 2919 (2004).
- [14] S. Banerji, M. Meem, A. Majumder, F. G. Vasquez, B. Sensale-Rodriguez, and R. Menon, *Optica* **6**, 805 (2019).
- [15] R. Peierls, *Ann. Phys. (Leipzig)* **395**, 1055 (1929).
- [16] S. Foteinopoulou and C. M. Soukoulis, *Phys. Rev. B* **72**, 165112 (2005).
- [17] P. St. J. Russell, T. A. Birks, and F. Dominic Lloyd-Lucas, in *Confined Electrons and Photons, New Physics and Applications*, edited by E. Burstein and C. Weisbuch, Vol. 340 of NATO Advanced Studies Institute, Series B: Physics (Plenum, New York, 1995), p. 585.
- [18] L. Brillouin, *Wave Propagation in Periodic Structures: Electric Filters and Crystal Lattices* (Courier Corporation, North Chelmsford, MA, 2003).
- [19] A. Yariv and A. Gover, *Appl. Phys. Lett.* **26**, 537 (1975).
- [20] A. A. Maznev and O. B. Wright, *Am. J. Phys.* **82**, 1062 (2014).
- [21] M. Minkov, I. A. D. Williamson, M. Xiao, and S. Fan, *Phys. Rev. Lett.* **121**, 263901 (2018).
- [22] S. L. Chuang, *Physics of Photonic Devices*, Vol. 80 (John Wiley & Sons, New York, 2012).
- [23] R. Zengerle, *J. Mod. Opt.* **34**, 1589 (1987).
- [24] D. Marcuse, *Theory of Dielectric Optical Waveguides* (Elsevier, New York, 2013).
- [25] W. Lu, Y. Huang, P. Vodo, R. Banyal, C. Perry, and S. Sridhar, *Opt. Express* **15**, 9166 (2007).
- [26] K. L. Tsakmakidis, A. D. Boardman, and O. Hess, *Nature* **450**, 397 (2007).
- [27] G. Chaplain, M. Makwana, and R. Craster, *Wave Motion* **86**, 162 (2019).
- [28] A. Colombi, D. Colquitt, P. Roux, S. Guenneau, and R. V. Craster, *Sci. Rep.* **6**, 27717 (2016).
- [29] A. Colombi, V. Ageeva, R. J. Smith, A. Clare, R. Patel, M. Clark, D. Colquitt, P. Roux, S. Guenneau, and R. V. Craster, *Sci. Rep.* **7**, 6750 (2017).
- [30] J. M. De Ponti, A. Colombi, R. Ardito, F. Braghin, A. Corigliano, and R. V. Craster, *New J. Phys.* **22**, 013013 (2020).
- [31] G. J. Chaplain and R. V. Craster, *Phys. Rev. B* **99**, 220102(R) (2019).
- [32] A. COMSOL, Comsol Multiphysics Reference Manual, version 5.3 (2008), [https://doc.comsol.com/5.3/doc/com.comsol.help.comsol/COMSOL\\_ReferenceManual.pdf](https://doc.comsol.com/5.3/doc/com.comsol.help.comsol/COMSOL_ReferenceManual.pdf).
- [33] H. O. Pierson, *Handbook of Chemical Vapor Deposition: Principles, Technology and Applications* (William Andrew, Norwich, NY, 1999).
- [34] A. Zhan, S. Colburn, R. Trivedi, T. K. Fryett, C. M. Dodson, and A. Majumdar, *ACS Photonics* **3**, 209 (2016).
- [35] R. H. Ritchie, *Phys. Rev.* **106**, 874 (1957).
- [36] J. B. Pendry, L. Martín-Moreno, and F. J. Garcia-Vidal, *Science (NY)* **305**, 847 (2004).
- [37] P. Muñoz, G. Micó, L. Bru, D. Pastor, D. Pérez, J. Doménech, J. Fernández, R. Baños, B. Gargallo, R. Alemany, A. M.

- Sánchez, J. M. Cirera, R. Mas, and C. Domínguez, *Sensors* **17**, 2088 (2017).
- [38] A. H. Ghadimi, S. A. Fedorov, N. J. Engelsen, M. J. Beryhi, R. Schilling, D. J. Wilson, and T. J. Kippenberg, *Science* **360**, 764 (2018).
- [39] R. E. Peierls, *Quantum Theory of Solids* (Clarendon, New York, 1996).
- [40] P. L. Taylor, P. L. Taylor, and O. Heinonen, *A Quantum Approach to Condensed Matter Physics* (Cambridge University Press, Cambridge, England, 2002).
- [41] See Supplemental Material at <http://link.aps.org/supplemental/10.1103/PhysRevB.101.155430> for extra examples, full dispersion curves, and method to remove spurious modes.
- [42] J. R. Wallbank, R. Krishna Kumar, M. Holwill, Z. Wang, G. H. Auton, J. Birkbeck, A. Mishchenko, L. A. Ponomarenko, K. Watanabe, T. Taniguchi, K. S. Novoselov, I. L. Aleiner, A. K. Geim, and V. I. Fal'ko, *Nat. Phys.* **15**, 32 (2019).
- [43] E. Bauer, *J. Chem. Phys.* **26**, 1440 (1957).
- [44] G. J. Chaplain, G. Macauley, J. Běllín, T. Tyc, E. N. Cowie, and J. Courtial, *J. Opt. Soc. Am. A* **33**, 962 (2016).
- [45] A. B. Constantine, *Antenna Theory: Analysis and Design* (Wiley-Interscience, New York, 2005).
- [46] A. A. Maradudin, *Structured Surfaces as Optical Metamaterials* (Cambridge University Press, Cambridge, England, 2011), Chap. 5, pp. 158–181.